PERGAMON

International Journal of Heat and Mass Transfer 44 (2001) 4075–4086

International Journal of HEAT and MASS TRANSFER

www.elsevier.com/locate/ijhmt

A theoretical model of brick drying as a conjugate problem

K. Murugesan [a], H.N. Suresh [b], K.N. Seetharamu [c], P.A. Aswatha Narayana [d,*], T. Sundararajan [e]

[a] *Department of Mechanical Engineering, K.R.E.C, Surathkal, India*
[b] *Department of Mechanical Engineering, P.E.S.C.E., Mandya 571 401, India*
[c] *Universiti Sains Malaysia, Perak Campus, Malaysia*
[d] *Department of Applied Mechanics, Fluid Mechanics Laboratory, Indian Institute of Technology, Chennai 600 036, India*
[e] *Department of Mechanical Engineering, Indian Institute of Technology, Chennai 600 036, India*

Received 11 July 1997; received in revised form 2 January 2001

Abstract

The evaporative drying of a two-dimensional rectangular brick is studied numerically as a conjugate problem. The conservation equations for the solid are obtained using the continuum approach. The Navier–Stokes equations have been employed for obtaining the flow field and the corresponding flow solutions are used for predicting the drying behavior of the brick. The predictions of temperature and moisture content show that the leading edge dries faster compared to other sides of the solid. The full two-dimensional solutions differ considerably from the solutions based on heat and mass transfer through the boundary layers over the top surface. Average heat and mass transfer coefficients appropriate to the conjugate problem have been defined, based on constant temperature and moisture differentials between the solid and the ambient. The corresponding Nusselt and Sherwood number values indicate that analogy does not exist between heat and mass transfer, until the entire brick reaches wet bulb conditions. Free convection effects on drying are also studied for some initial period for low Reynolds number. Due to the influence of buoyant forces imparted by gravity, the overall drying rate has improved.

1. Introduction

The binder removal process from clay products is very critical and has to be considered for the following reasons: (i) excess water present in the product may cause firing faults, (ii) the heat of vaporization is enormous when the binder removal is carried out in a dryer. The wet products have to be dried to their equilibrium moisture for the given ambient conditions. Based on the theory of drying proposed by Luikov [1] and later by Whitaker [2], many mathematical models for drying of porous materials have been developed. The overall drying process of a solid can be viewed as the removal of free water content as well as the bound water. The free water is removed during the constant rate period in which the moisture transfer occurs due to capillary forces. When the surface moisture reduces to such an extent that the continuity of water flow by capillary action is disrupted, the rate of drying starts decreasing. Now the moisture evaporates within the solid itself and diffuses towards the surface and this period is called as the falling rate drying period. Nasrallah and Perre [3] and Huang [4] used different models for the constant and falling rate drying periods. Kallel et al. [5] used a unified model based on Whitaker's [2] theory, with diffusion coefficients varying as functions of moisture content for the entire drying period. The above one-dimensional and two-dimensional models [6,7] employed heat and mass transfer coefficients from available correlations, which were obtained using boundary layer equations.

In reality, drying is a conjugate problem. Also the process is transient in nature wherein the resistances for heat and mass transfer at the interface vary with time. Hence, the heat and moisture transfer within the porous solid have to be studied along with the transport

* Corresponding author. Tel.: +91-4458173; fax: +91-2350509.
E-mail address: paan@iitm.ac.in (P.A. Aswatha Narayana).

0017-9310/01/$ - see front matter
PII: S0017-9310(01)00065-5

Nomenclature

A	area normal to the x or y direction (m^2)
C	specific heat capacity (J/kg K); concentration (kg/m^3)
C^*	equivalent specific heat (J/kg K)
D	diffusion coefficient (m^2/s)
D_m	isothermal diffusion coefficient (m^2/s)
D_T	non-isothermal diffusion coefficient (m^2/K s)
H	enthalpy (J/kg); height (m)
h_c	convective heat transfer coefficient (W/m^2 K)
h_m	convective mass transfer coefficient (m/s)
J	mass flux (kg/m^2 s)
k	thermal conductivity (W/m K); node of an element
L	length (m)
M	mass (kg)
N	shape function
m	rate of phase change (kg/s)
p	pressure (Pa)
Re	Reynolds number based on the height of the brick ($Re = \rho U_\alpha H_b/\mu$)
t	time (s)
T	temperature (K)
u	velocity in the x direction (m/s)
v	velocity in the y direction (m/s)
U_α	free stream velocity (m/s)
w	moisture content in liquid or vapor phase (kg/kg of dry solid)
W	total moisture content ($= w_l + w_v$)
x, y	spatial coordinates

Greek symbols

μ	coefficient of dynamic viscosity (Pa s)
ϕ	relative humidity
β	coefficient of thermal expansion (K^{-1})
β^*	coefficient of expansion with concentration (m^3/kg)
ρ	mass density (kg/m^3)

Subscripts

b	brick
c	corresponding to constant differences in temperature and concentration
f	fluid or flow domain
i	initial conditions in the slab; node of an element
j	mobile component (dry air, liquid or vapor); node of an element
l	liquid
o	dry porous solid
s	surface conditions
t	based on instantaneous temperature and concentration differences
v	vapor
w	moisture (either liquid or vapor)
α	ambient conditions

processes in the drying medium. Dolinsky et al. [8] studied the convective drying of materials like paper and found that the solution of conjugate problem yields lesser drying rate values than those obtained by decoupled analyses. It was also shown that the frequently assumed analogy between heat and mass transfer coefficients may not exist in reality. Masmoudi and Prat [9] studied the conjugate drying of unsaturated sand and found that analogy holds good for heat and mass transfer coefficients only for the initial period of drying. For the later part of drying, the heat and mass transfer coefficients at the interface may differ from standard values obtained through correlations due to the non-uniformity of moisture and temperature distributions at the interface resulting from conjugate nature of transfers.

Zeghmati and Daguenet [10] observed from their study of conjugate drying of pinewood that the average Nusselt and Sherwood numbers are highly affected by the internal vapor diffusion. However, the vapor velocity at the wall does not affect the gas-phase transport processes significantly and hence the assumption of zero vapor velocity at the wall is justified for external flow analysis, at least in the limit of low drying rates. Oliveira and Haghighi [11] obtained the temperature and moisture contours for the drying of wood, considering a laminar boundary layer flow over the solid. They used the adaptive finite element technique to solve the governing equations for the solid and the fluid.

In all the above studies, the conjugate problems have been solved using only boundary layer equations for the flow domain. The sides of the solid are taken to be adiabatic. Such an approximation may be sufficient to analyze the drying of long objects like wooden logs, since the convective drying from the top surface of the solid is only of interest. But the drying of rectangular brick is a three-dimensional problem. The study of three-dimensional conjugate problem is a complex one. Also even for two-dimensional conjugate studies results are available only with boundary layer equations for the flow field. Hence in the present study, as a first attempt to bring out the limitations of use of boundary layer equations, a two-dimensional conjugate analysis of brick drying is considered, using Navier–Stokes equations for the flow field including the buoyancy terms. The present two-dimensional conjugate analysis may hold good for

situations where the number of bricks are stacked one behind the other, with small gap between adjacent bricks. Furthermore, most of the earlier conjugate studies have considered only few hours of drying, covering only the initial drying period till the boundary layers are established.

In the present work, two-dimensional Navier–Stokes equations (including buoyancy terms) are solved for the flow domain, coupled with the energy and moisture transport equations for brick. The results are presented here for 36 h of drying by which time the brick reaches the wet bulb temperature for the given ambient conditions.

2. Mathematical model

Air with a uniform free stream velocity of U_∞ is assumed to flow over a rectangular brick of aspect ratio 2 placed on a flat surface (Fig. 1). The brick is assumed to be saturated with water. Initially, the temperature of the brick is the same as that of air and the concentration difference between the brick surface and the ambient causes water to evaporate from the brick. This results in the reduction of brick surface temperature. As drying proceeds with time, the solid reaches the wet bulb temperature corresponding to the given ambient conditions and remains at this temperature for a significantly long period of time. Finally, the brick gets heated up as heat flows from air to the brick. The flow conditions and properties employed in the computations of the present study are given in Table 1.

2.1. Governing equations for the porous solid

The two-dimensional conservation equations for liquid and vapor in the porous solid are obtained using the continuum approach [5] as follows:

Liquid

$$\frac{\partial w_\mathrm{l}}{\partial t} = -\frac{1}{\rho_0}\left[\frac{\partial J_{\mathrm{l}x}}{\partial x} + \frac{\partial J_{\mathrm{l}y}}{\partial y}\right] + \frac{\dot{m}}{M_0}. \tag{1}$$

Vapor

$$\frac{\partial w_\mathrm{v}}{\partial t} = -\frac{1}{\rho_0}\left[\frac{\partial J_{\mathrm{v}x}}{\partial x} + \frac{\partial J_{\mathrm{v}y}}{\partial y}\right] - \frac{\dot{m}}{M_0}. \tag{2}$$

In the above equations, J denotes the diffusion flux of moisture and w represents the moisture content per kg of dry solid.

The energy equation is

$$\rho_0 \frac{\partial}{\partial t}\left(\Sigma w_j H_j\right) = \frac{\partial}{\partial x}\left(k\frac{\partial T}{\partial x}\right) + \frac{\partial}{\partial y}\left(k\frac{\partial T}{\partial y}\right) - \frac{\partial}{\partial x}\left(\Sigma J_j H_j\right) - \frac{\partial}{\partial y}\left(\Sigma J_j H_j\right), \tag{3}$$

where j represents l or v, corresponding to liquid and vapor phases, respectively.

Using Darcy's law for capillary liquid mass flux and Fick's law for diffusive mass flux, the final continuity equations for liquid and vapor are:

Liquid

$$\frac{\partial w_\mathrm{l}}{\partial t} = \frac{\partial}{\partial x}\left[D_\mathrm{ml}\frac{\partial W}{\partial x} + D_\mathrm{Tl}\frac{\partial T}{\partial x}\right] + \frac{\partial}{\partial y}\left[D_\mathrm{ml}\frac{\partial W}{\partial y} + D_\mathrm{Tl}\frac{\partial T}{\partial y}\right] + \frac{\dot{m}}{M_0}. \tag{4}$$

Vapor

$$\frac{\partial w_\mathrm{v}}{\partial t} = \frac{\partial}{\partial x}\left[D_\mathrm{mv}\frac{\partial W}{\partial x} + D_\mathrm{Tv}\frac{\partial T}{\partial x}\right] + \frac{\partial}{\partial y}\left[D_\mathrm{mv}\frac{\partial W}{\partial y} + D_\mathrm{Tv}\frac{\partial T}{\partial y}\right] - \frac{\dot{m}}{M_0}, \tag{5}$$

where D_ml, D_Tl, D_mv, D_Tv represent the isothermal and non-isothermal diffusion coefficients for liquid and vapor, respectively.

Summing up Eqs. (4) and (5) and neglecting the vapor accumulation (since $w_\mathrm{v} \ll w_\mathrm{l}$ for a major part of the drying period), the expression for moisture conservation is given by

$$\frac{\partial w}{\partial t} = \frac{\partial}{\partial x}\left[(D_\mathrm{mv}+D_\mathrm{ml})\frac{\partial W}{\partial x} + (D_\mathrm{Tv}+D_\mathrm{Tl})\frac{\partial T}{\partial x}\right] + \frac{\partial}{\partial y}\left[(D_\mathrm{mv}+D_\mathrm{ml})\frac{\partial W}{\partial y} + (D_\mathrm{Tv}+D_\mathrm{Tl})\frac{\partial T}{\partial y}\right] \tag{6}$$

and the rate of vapor condensation is given by

$$\frac{\dot{m}}{M_0} = \frac{\partial}{\partial x}\left[D_\mathrm{mv}\frac{\partial w_\mathrm{l}}{\partial x} + D_\mathrm{Tv}\frac{\partial T}{\partial x}\right] + \frac{\partial}{\partial y}\left[D_\mathrm{mv}\frac{\partial w_\mathrm{l}}{\partial y} + D_\mathrm{Tv}\frac{\partial T}{\partial y}\right]. \tag{7}$$

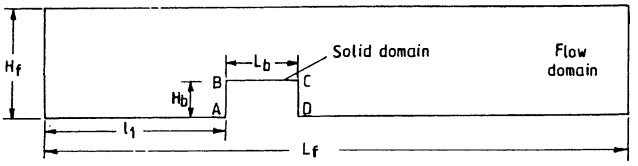

Fig. 1. Schematic diagram of computational domain.

Table 1
Data used in computations

(i) Flow conditions		
$T_\alpha = 293.0$ K, $U_\alpha = 1.8$ m/min, $\phi = 50\%$		
(ii) Initial conditions for brick		
$T_i = 293.0$ K, $W_i = 0.13$ kg/kg of dry solid		
(iii) Dimensions		
$L_f = 1.6$ m, $H_f = 0.3$ m; $L_b = 0.2$ m, $H_b = 0.1$ m		
(iv) Properties		
	Brick	Gas phase
ρ (kg/m^3)	1800.00	1.21
C_p (J/kg K)	1200.00	1.0056E03
k (W/m K)	1.8	0.02568
μ (Pa s)	–	1.8116E − 05
D (m^2/s)	–	0.256E − 04
D_{ml} (m^2/s)	1.0E − 08[a]	–
D_{Tl} (m^2/K s)	1.0E − 12[a]	–
D_{mv} (m^2/s)	1.0E − 12[a]	–
D_{Tv} (m^2/K s)	1.0E − 12[a]	–

[a] At average moisture content of solid [5].

The energy equation within the porous solid can be simplified by dropping the convective term, since convective heat transfer through the solid is very small compared to heat transfer due to diffusion and phase change. Hence Eq. (3) becomes

$$C^* \frac{\partial T}{\partial t} = \frac{1}{\rho_0}\left[\frac{\partial}{\partial x}\left(k\frac{\partial T}{\partial x}\right) + \frac{\partial}{\partial y}\left(k\frac{\partial T}{\partial y}\right)\right] + \frac{\dot{m}}{M_0}(H_v - H_l), \tag{8}$$

where the equivalent specific heat capacity of the porous solid is determined as

$$C^* = C_0 + w_l C_l + w_v C_v.$$

Gravitational effects on moisture transfer are not taken into account. For a brick of the size considered in the present effort, gravitational effects are completely negligible compared to capillary effects. The transport properties of the solid occurring in the above governing equations are strong functions of moisture content. These properties must be measured experimentally for a given solid. In the present analysis, however, constant transport properties evaluated at average moisture content of the solid have been employed, with the primary objective of highlighting two dimensional convective effects upon the drying process. Consequently, the simplified energy equation for the porous solid is obtained as

$$\frac{\partial T}{\partial t} = K_1\left[\frac{\partial}{\partial x}\left(\frac{\partial T}{\partial x}\right) + \frac{\partial}{\partial y}\left(\frac{\partial T}{\partial y}\right)\right] + K_2\left[\frac{\partial}{\partial x}\left(\frac{\partial W}{\partial x}\right) + \frac{\partial}{\partial y}\left(\frac{\partial W}{\partial y}\right)\right], \tag{9}$$

where

$$K_1 = \left[\frac{k}{\rho_0 C^*} + \frac{(H_v - H_l)D_{Tv}}{C^*}\right]; \quad K_2\frac{(H_v - H_l)}{C^*}.$$

The moisture conservation equation (6) can also be rewritten as

$$\frac{\partial W}{\partial t} = K_3\left[\frac{\partial}{\partial x}\left(\frac{\partial W}{\partial x}\right) + \frac{\partial}{\partial y}\left(\frac{\partial W}{\partial y}\right)\right] + K_4\left[\frac{\partial}{\partial x}\left(\frac{\partial T}{\partial x}\right) + \frac{\partial}{\partial y}\left(\frac{\partial T}{\partial y}\right)\right], \tag{10}$$

where

$$K_3 = (D_{mv} + D_{ml}); \quad K_4 = (D_{Tv} + D_{Tl}).$$

Eqs. (9) and (10) represent the coupled transport equations for the solid.

2.2. Governing equations for the flow field

For the flow domain, the Navier–Stokes equations, energy equation and the moisture transport equation are given by:

Continuity

$$\frac{\partial u}{\partial x} + \frac{\partial v}{\partial y} = 0, \tag{11}$$

x-momentum

$$\frac{\partial u}{\partial t} + u\frac{\partial u}{\partial x} + v\frac{\partial u}{\partial y} = -\frac{1}{\rho_f}\frac{\partial p}{\partial x} + \frac{\mu}{\rho_f}\left[\frac{\partial^2 u}{\partial x^2} + \frac{\partial^2 u}{\partial y^2}\right], \tag{12}$$

y-momentum

$$\frac{\partial v}{\partial t} + u\frac{\partial v}{\partial x} + v\frac{\partial v}{\partial y} = -\frac{1}{\rho_f}\frac{\partial p}{\partial y} + \frac{\mu}{\rho_f}\left[\frac{\partial^2 v}{\partial x^2} + \frac{\partial^2 v}{\partial y^2}\right] + g\beta(T - T_\infty) + g\beta^*(C - C_\infty), \tag{13}$$

where $g\beta(T - T_\infty)$ and $g\beta^*(C - C_\infty)$ represent the buoyancy terms due to temperature and concentration gradients.

Energy equation

$$\frac{\partial T}{\partial t} + u\frac{\partial T}{\partial x} + v\frac{\partial T}{\partial y} = \frac{k}{\rho_f C_{pf}}\left[\frac{\partial^2 T}{\partial x^2} + \frac{\partial^2 T}{\partial y^2}\right] \tag{14}$$

Concentration equation

$$\frac{\partial C}{\partial t} + u\frac{\partial C}{\partial x} + v\frac{\partial C}{\partial y} = D\left[\frac{\partial^2 C}{\partial x^2} + \frac{\partial^2 C}{\partial y^2}\right] \tag{15}$$

The boundary conditions at the air–porous solid interface are given as follows:

No slip

$$u = 0, v = 0,$$

Temperature continuity

$$T_f = T_s, \tag{16}$$

Moisture continuity

$$C_f = C(T, W)_s, \tag{17}$$

Heat balance

$$[k + (H_v - H_l)D_{Tv}]\frac{\partial T}{\partial n} + (H_v - H_l)D_{mv}\frac{\partial W}{\partial n} = K_f\frac{\partial T_f}{\partial n} + (H_v - H_l)D\frac{\partial C_f}{\partial n},$$

where D is the diffusion coefficient for vapor in air medium.

Species flux balance

$$D_{Tv}\frac{\partial T}{\partial n} + D_{mv}\frac{\partial W}{\partial n} = D\frac{\partial C_f}{\partial n}.$$

The gas-phase boundary conditions are:

At inlet ($x = 0$),

$$u = U_\alpha, v = 0, T = T_\alpha \text{ and } C = C_\alpha,$$

In the far stream ($y = H_f$),

$$u = U_\alpha, T = T_\alpha, \text{ and } C = C_\alpha.$$

Smooth extrapolation is used at the outflow boundary ($x = L_f$) and the bottom boundary is taken as adiabatic.

3. Finite element formulation

Finite element spatial discretization of the governing equations is performed by the Galerkin's weighted residual method. Triangular elements are used to represent the variables of the gas phase and the porous solid. Within each element, the variables are represented in terms of their nodal values through the expression

$$\phi = N_i\phi_i + N_j\phi_j + N_k\phi_k,$$

where ϕ is any flow or transport variable and N_i, N_j, N_k are the nodal shape functions.

Eqs. (9)–(15) are integrated using the respective shape functions as weighting functions.

The solution of momentum equations is obtained using the Eulerian velocity correction method [12]. The algorithm has the following steps:

(i) calculation of pseudo-velocities, neglecting the pressure terms in the x and y momentum equations
(ii) evaluation of pressure from pressure Poisson equation
(iii) correction of the pseudo velocities to get actual velocities.

As pointed out by Masmoudi and Prat [9], the characteristic time scale of the flow field is much smaller compared to the time scale of the heat and moisture transfer within the brick. Hence the flow field is assumed to be in a quasi-steady-state condition.

The transient solutions of the energy and concentration equations (14) and (15) are obtained using the velocities corresponding to steady flow. A five-point fit for temperature and concentration is used to calculate the fluxes at the interface at a given time, using the temperature and moisture continuity equations (16) and (17), respectively. The concentration of the fluid at the interface can be determined from the local relative humidity, which is obtained using Henderson's modified desorption isotherm (Mauri Fortes and Martin R. Okos, [13]) of the form as given below

$$\phi = 1 - \exp(-17W^{0.6}).$$

The constants in the above expression are obtained by trial and error, to satisfy the equilibrium moisture content value of 0.005 kg/kg of dry solid at 50% relative humidity, used by Kallel et al. [5] for the brick considered in the present study.

The conservation equations for the solid, (9) and (10), are now solved with these surface fluxes as boundary conditions. With known temperature and concentration at the surface of the solid, the energy and concentration equations of the gas phase are solved for the next time step. This explicit time marching procedure is continued until a significant drop in moisture content of the solid occurs. The CPU time taken for simulating 36 h of drying process is 252 h on an IBM-RS 6000 machine.

4. Results and discussion

A grid sensitivity study has been carried out for the computational domain shown in Fig. 1. The average Nusselt and Sherwood numbers over the left, top and right sides of the solid have been calculated for determining the variations of the numerical solutions due to computational grid. Three different meshes with 2800, 3712 and 4465 nodes (5316, 7098 and 8576 elements, repectively) have been employed. Small step sizes are used near the solid surface where the gradients are maximum.

The change in the average Nusselt and Sherwood numbers was found to be 3.4% between meshes I & II and 1.8% between meshes II & III. Hence the third mesh with 4465 nodes and 8576 elements was chosen for all the predictions of the conjugate drying problem (Fig. 2).

Detailed experimental data are not available for validating the simulation of conjugate heat and mass transfer associated with brick drying. Therefore, the different modules of the conjugate calculation procedure have been validated individually. For instance, two-dimensional flow calculations over a square block have been compared with the results of Yang and Atluri [14] for a similar geometry. For flow Reynolds number equal

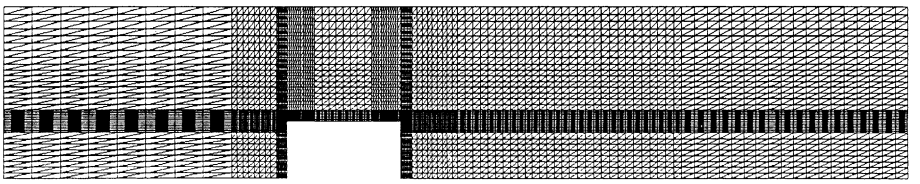

Fig. 2. Computational mesh.

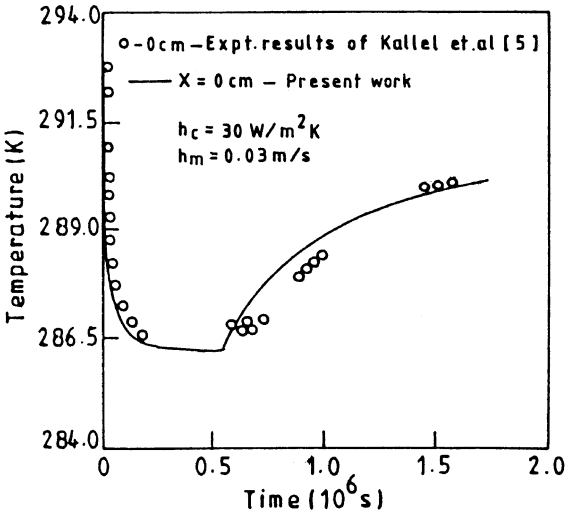

Fig. 3. Experimental comparison of one-dimensional results.

to 200, the length of the recirculation zone predicted in the present work agrees with the result obtained by Chien-Tung Yang and Satya [14] within 1%. As regards porous solid drying, experimental results are available (Kallel et al. [5]), for the one dimensional drying situation. By setting adiabatic conditions on the side surfaces and prescribing convective heat and mass transfer coefficients for the top surface, numerical results have been simulated [15]. These are compared with the experimental results in Fig. 3. In the computations of the present study, constant transport properties evaluated at average moisture content of the solid have been used for the entire drying period (Kallel et al. [5], Perrin and Javelas [16]).

Oliveira and Haghighi [11] have studied the convective drying of wood by the conjugate approach based on Luikov's equations. Insulated side surfaces and convective heat and mass transfer from the top surface were considered by these authors. The same problem has been simulated in the present study and the predicted results are in qualitative agreement with those of Oliveira and Haghighi [11] as shown in Figs. 4 and 5. The differences in temperature distributions between the full two-dimensional results and boundary layer results are small, compared to the differences in the moisture content distributions. This may be because the models used in the two works are different and all the transport properties required for the present model are not available. Furthermore, since boundary layer equations were used by Oliveira and Haghighi [11], the effect of convective drying on the left and right sides of the solid was not predicted. In the present study, the top, left and right sides are also subjected to convective boundary conditions. A comparison between the results of full two-dimensional predictions and convective drying only through the top surface is shown in Figs. 4 and 5. It is observed that the gradients of temperature and moisture content are larger at the leading edge, with the left side taking a predominant part in the drying process. The deviations between the full two-dimensional and boundary layer predictions are seen to increase away

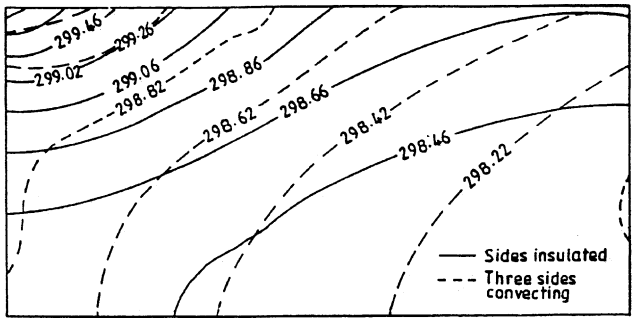

Fig. 4. Temperature contours for wood at 2 h for timber drying analysis at $Re = 200$ ($T_i = 298.0$ K, $T_j = 333.0$ K, $W_i = 0.45$ kg/kg of dry solid, $\varphi = 10\%$).

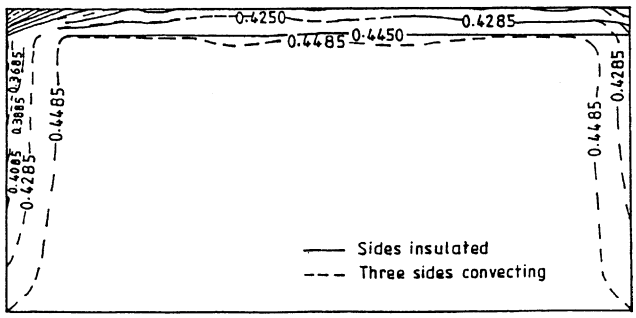

Fig. 5. Comparison of moisture contours at 2 h for timber drying.

from the leading edge. Also the variations of average moisture content with time are computed using both conjugate and boundary layer models in order to highlight the conjugate effect. These results are obtained for a rectangular brick of size 0.2×0.1 m with an initial moisture content of 0.13 kg/kg of dry solid and a temperature of 293.0 K when it undergoes evaporative drying by air with 50% relative humidity under forced convection conditions and are shown in Fig. 6. The average moisture content for boundary layer model is calculated with heat and mass transfer coefficient values ($2\ W/m^2\ K$ and $0.02\ m/s$) obtained using standard correlations for a Reynolds number value of 200. The solid line in Fig. 6 indicates the results obtained from the conjugate model. As can be seen from the above figure, the use of constant values of heat and mass transfer coefficients overpredicts the moisture removal. For the same brick under the same drying conditions the conjugate drying results for mixed and forced convection cases are discussed in the following sections.

4.1. Results for the drying of brick under mixed convection condition

The conjugate drying results for temperature distribution along the surfaces of the solid for mixed convection are shown in Fig. 7 at the end of 1, 12, 24 and 36 h. Here A, B, C and D represent the corners of the two-dimensional brick block (Fig. 1). During the initial period of drying, the surface temperature of the solid decreases since the heat required for vaporization is absorbed partially from the solid itself. It is also observed that the temperature drop at the leading edge B is more compared to other regions, due to the development of a thin thermal boundary layer over the top surface. As drying proceeds with time, heat flows from air to the solid by convection because of the temperature difference between the solid surface and air. However, the heat of vaporization is still more than the available convective heat flux from the ambient and the surface temperature continues to decrease even upto 36 h of

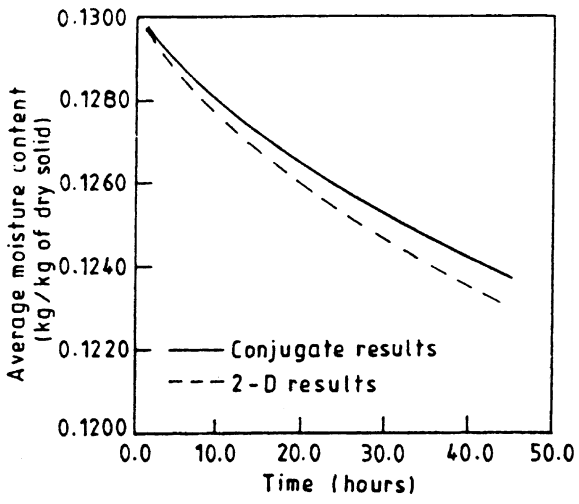

Fig. 6. Comparison of average moisture content between conjugate and two-dimensional results.

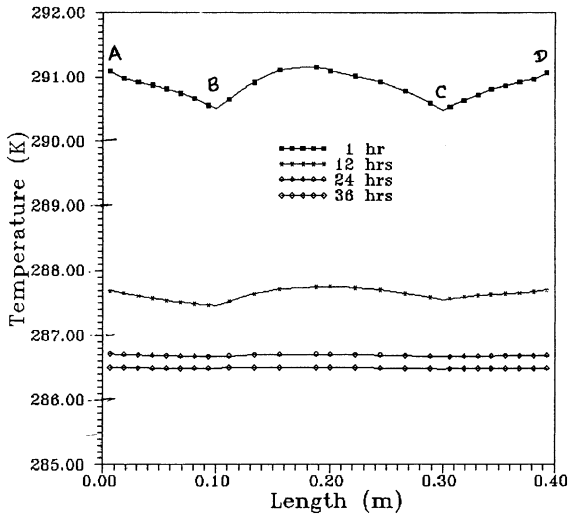

Fig. 7. Temperature distribution along surface of the brick for mixed convection.

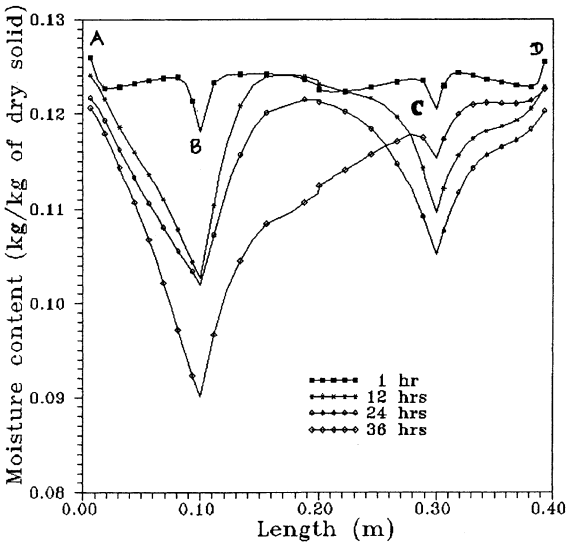

Fig. 8. Moisture distribution along surface of the brick for mixed convection.

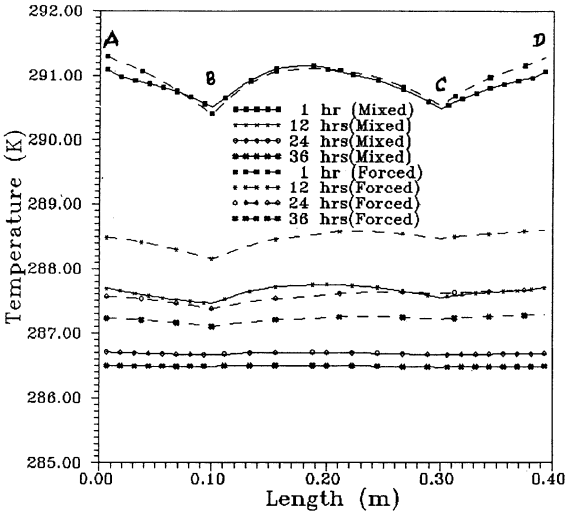

Fig. 9. Comparison of temperature distribution between mixed and forced convections.

drying, as seen from Fig. 7. After sufficient passage of time, the temperature within the entire solid is reduced to a uniform value corresponding to the wet bulb temperature.

The distribution of moisture content over the brick surface is shown in Fig. 8. It is observed that the rate of evaporation is high at the leading edge compared to other regions because of the development of a thin concentration boundary layer. However, the evaporation rate decreases with time, as the concentration difference between the ambient and the solid surface decreases. When the solid attains uniform temperature around 36 h, significant moisture gradients still exist within the solid. This is because the resistance for moisture transfer through the solid is more compared to that for heat transfer owing to the relatively smaller diffusion coefficient value for mass transfer.

4.2. Comparison between mixed and forced convection results

The conjugate drying results are also obtained for forced convection case by ignoring the buoyancy terms in Eq. (13). Fig. 9 shows the comparison of temperature distribution along the surfaces of brick between mixed and forced convection cases. The solid lines represent the results for mixed convection case. At the end of 1 h the temperature drop at the leading and trailing edges of the brick for mixed convection case is more than that of the forced convection case due to the buoyancy effect. Also the solid reaches the wet bulb temperature much earlier in the mixed convection case. The moisture distributions along the surfaces of the brick are also compared between the mixed and forced convection cases and are shown in Fig. 10. The drop in moisture content at the leading edge B is much greater in the case of mixed convection compared to the forced convection case. The effect of buoyancy terms can be well understood by plotting the variations of average moisture content of the solid with time as shown in Fig. 11. The amount of moisture removed at a given time is more in the case of mixed convection case compared to the forced convection case. This trend can also be

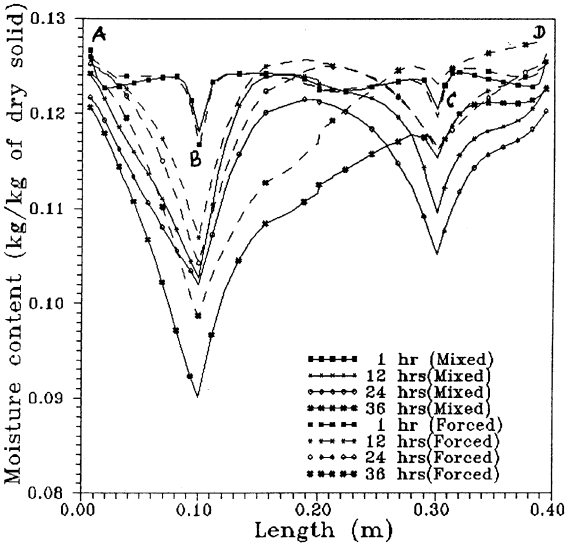

Fig. 10. Comparison of moisture distribution between mixed and forced convections.

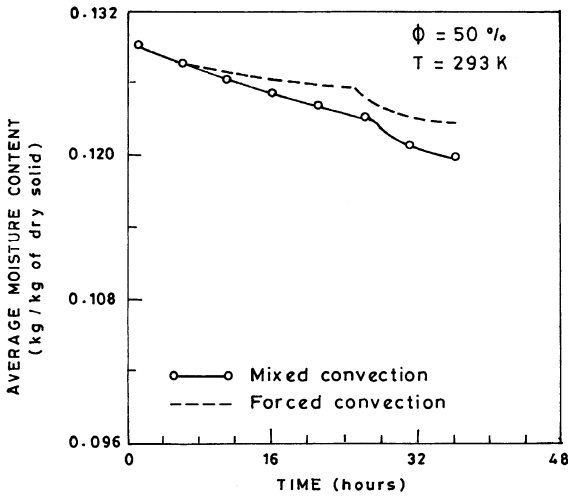

Fig. 11. Comparison of time evolution of average moisture content between mixed and forced convections.

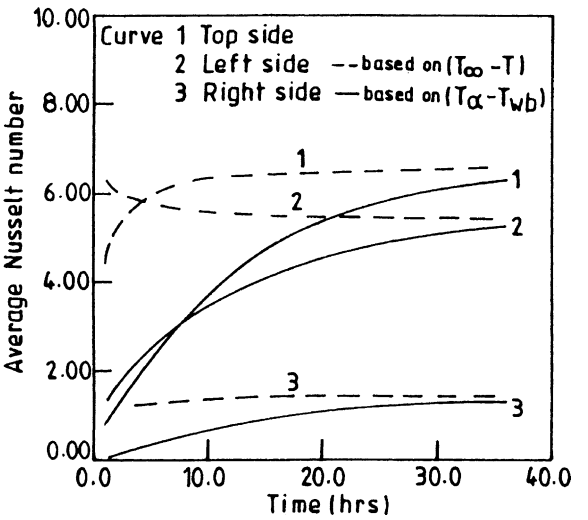

Fig. 13. Variation of average Nusselt number with time for forced convection.

interpreted as the increase in rate of drying as shown in Fig. 12.

Drying is a transient phenomenon in which the resistances for heat and mass transfer at the interface of the solid vary with time. Assuming the thermal conductivity and diffusion coefficient to be constant for the drying medium, the convective heat and mass transfer resistances can be represented in terms of variations of *Nu* and *Sh* with time. Of course, these variations correspond to only one set of initial conditions of the brick. But the trends of *Nu* and *Sh* will remain the same for the given flow situations. The temporal variations of average Nusselt and Sherwood numbers over the surfaces of the solid for forced convection case are shown in Figs. 13 and 14, respectively. An important point to be noted here is that the surface heat and mass transfer coefficients depend upon the temperature or moisture potential differences considered in their definition. For instance, one could employ the instantaneous T or C between the solid surface and the ambient. However, heat and mass transfer coefficients derived in this fashion may not be very useful. Since a major part of the drying process occurs close to the wet bulb condition of the brick, it is possible to define the heat and mass transfer coefficients with respect to constant potentials $(T_\alpha - T_{wb})$ and

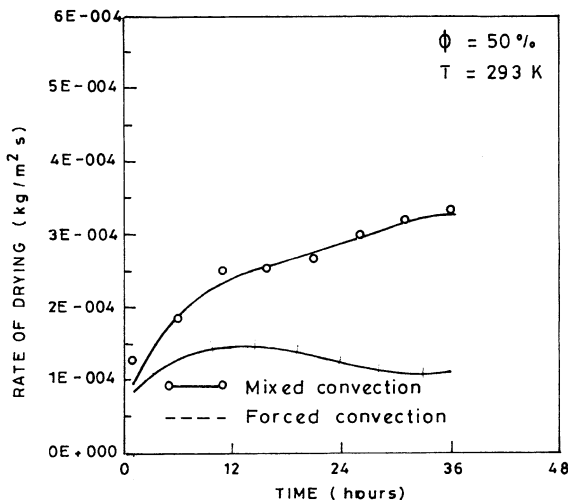

Fig. 12. Comparison of rate of drying between mixed and forced convections.

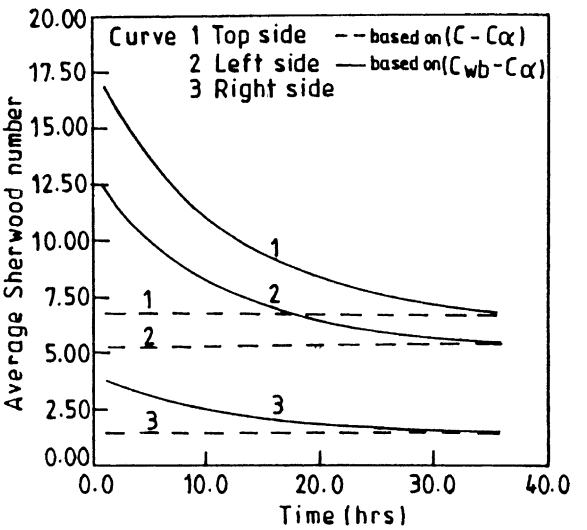

Fig. 14. Variation of average Sherwood number with time for forced convection.

($C_\alpha - C_{wb}$). Such a definition incorporates the conjugate nature of heat and mass transfer during drying.

In Fig. 13, the solid lines represent the average Nusselt number (Nu_c) based on the difference between the dry bulb and wet bulb temperatures (at 50% relative humidity and 293.0 K). The dotted lines represent the average Nusselt number (Nu_t) based on the instantaneous temperature difference between the ambient and the solid surface. Similarly in Fig. 14 the solid lines represent the average Sherwood number (Sh_c) based on the moisture potential difference ($C_{wb} - C_\alpha$) and dotted lines correspond to the average Sherwood number (Sh_t) based on the instantaneous concentration difference. In both the figures, Nu_c and Sh_c asymptotically approach the values of Nu_t and Sh_t, respectively, as expected. In Fig. 13, it is observed that Nu_t is constant for most of the period under consideration, except for the initial duration when the boundary layers are established. The corresponding heat transfer coefficient is primarily a function of the steady-state flow field. The value of Nu_c, however, increases with time since it incorporates the variation of the temperature difference ($T_s - T_\alpha$) until the wet bulb condition is reached. As for the Sherwood number variations shown in Fig. 14, it is seen Sh_t is constant for most of the drying period, for reasons similar to those for Nu_t. On the other hand, Sh_c decreases with time due to diminishing moisture potential. An important feature which is evident from these figures is that the analogy between heat and mass transfer is applicable to a reasonable accuracy (i.e., $Sh_c > Nu_c$) only after wet bulb conditions are reached. Until then, the rate of heat transfer to the block increases with time, while the evaporation rate decreases.

As an attempt to check the model for predictions during the initial drying period, drying results were obtained for a short duration of time for forced convection case. A closer look at the initial drying phenomenon is presented in Fig. 15, by plotting Nu_t (Nusselt number based on the difference between the ambient and the solid surface at the given instant) and Sh_t (Sherwood number based on the difference between the concentration in the ambient and the concentration at the solid surface at the given instant) for a short duration ($t < 90$ s). The establishment of thermal and concentration boundary layers is evident within this period. It is also observed by comparing Figs. 15 and 13 that for the top surface, Nu_t decreases rapidly in the beginning, then it increases and finally becomes constant with the elapse of time. These trends are in complete conformity with the results of Zeghmati et al. [10] for the drying of a wet plate. Zeghmati et al. [10] attributed the initial rapid decrease and subsequent increase of Nu_t to the predominance of diffusive phenomena during the estab-

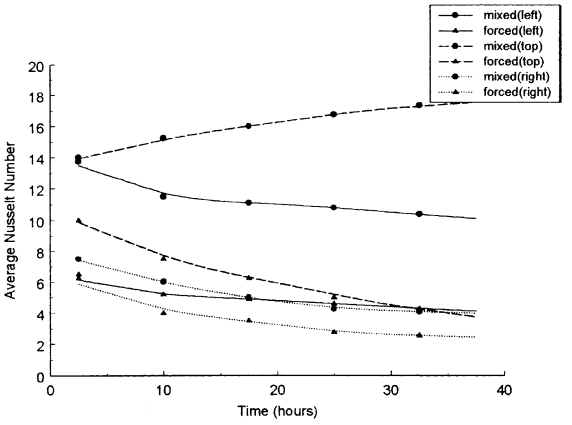

Fig. 16. Comparison of time evolution of Nusselt numbers between mixed and forced convections.

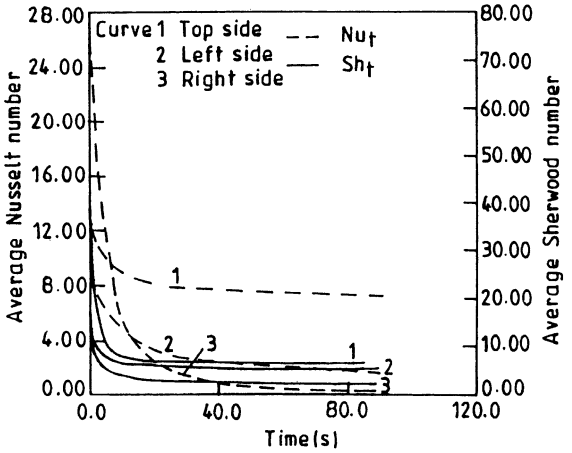

Fig. 15. Variation of Nusselt and Sherwood numbers during initial transient period for forced convection.

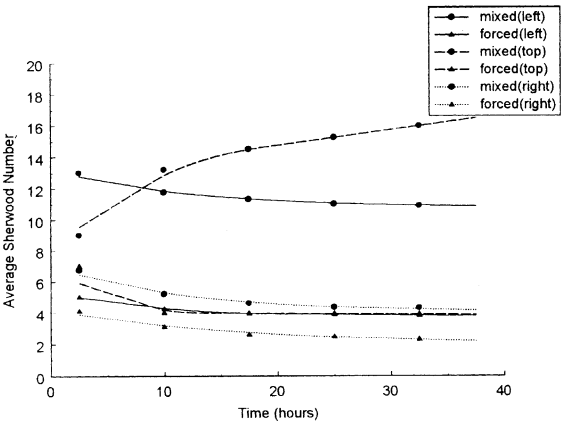

Fig. 17. Comparison of time evolution of Sherwood numbers between mixed and forced convections.

lishment of the boundary layer and the importance of convection for the subsequent period. The present predictions indicate that Nu_t values over the side surfaces continuously decrease with time. As regards mass transfer, the full two-dimensional results depict only the initial rapid decrease and there is no noticeable increase in Sh_t with time, in contrast to the observations of Zeghmati et al. [10] for a flat plate.

The comparison between the time evolution of average Nusselt and average Sherwood numbers for mixed and forced convection cases is shown in Figs. 16 and 17, respectively. The average Nusselt number (Nu_c) is based on the difference between the dry bulb and wet bulb temperatures (at 50% relative humidity and 293.0 K). Similarly the average Sherwood number (Sh_c) is based on the moisture potential difference ($C_{wb} - C_\infty$). In the above two figures, all the lines with circle represent the results for mixed convection case and the lines with triangle represent the results for forced convection case. The resistance for heat and mass transfer at the leading edge and hence on the top surface of the brick decrease due to the thin boundary layer effect. This is further enhanced due to the buoyancy term in the mixed convection case. These trends are depicted clearly by the continuous increase in the values of average Nusselt and Sherwood numbers as shown in Figs. 16 and 17. The resistance for heat and mass transfer at the left and right sides of the brick are more due to the stagnation and

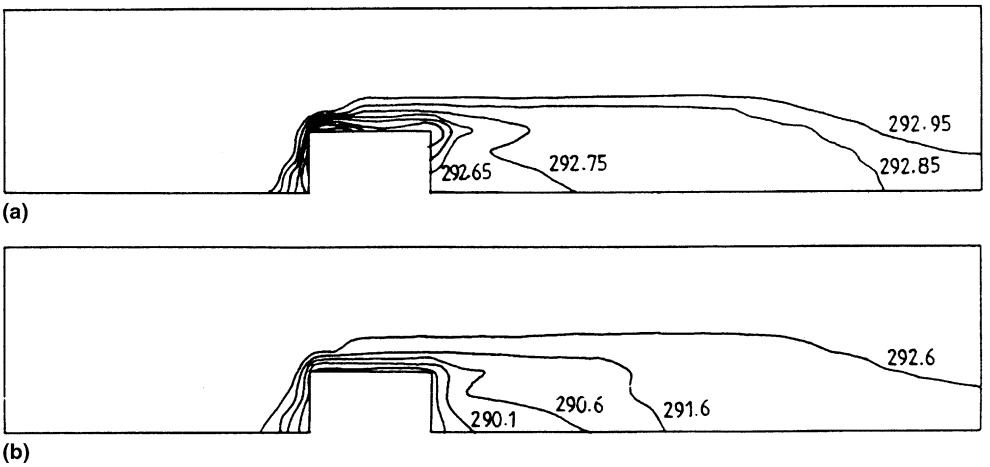

Fig. 18. (a) Temperature (K) contours in the flow field at 1 h for forced convection; (b) temperature (K) contours in the flow field at 36 h for forced convection.

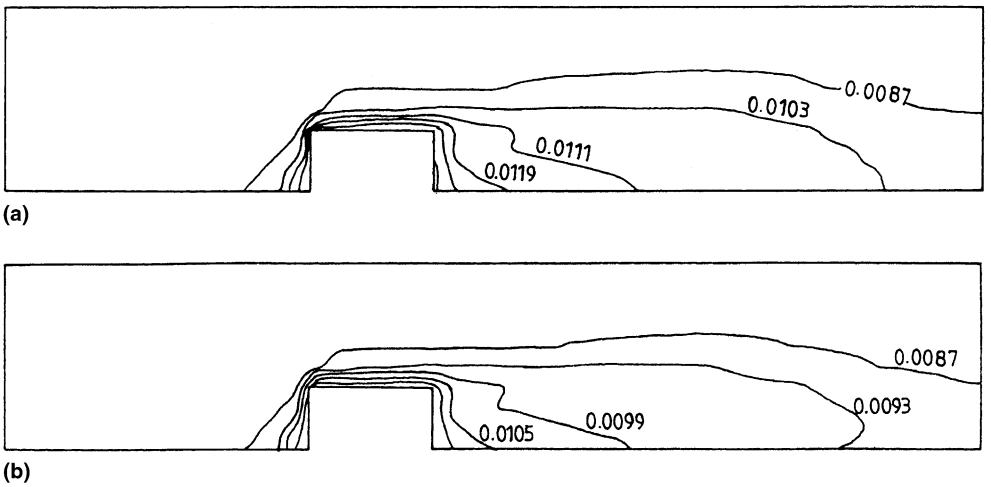

Fig. 19. (a) Moisture contours (kg/kg of dry air) in the flow field at 1 h for forced convection; (b) moisture contours (kg/kg of dry air) in the flow field at 36 h for forced convection.

recirculation effects, respectively. The higher values of Nusselt and Sherwood number for left and right sides for mixed convection case indicate that the resistance in mixed convection case is lower compared to that in forced convection case due to the buoyancy effect.

The gas-phase temperature and moisture contours at different time instants are shown in Figs. 18 and 19, respectively. The figures illustrate that after the establishment of the boundary layers, the changes in heat and mass transfer processes are rather slow. However, the temperature field evolves relatively faster than the moisture concentration field. It is also evident that while bulk of the heat and mass transfer occur through the top surface, the side surfaces also participate to some extent.

5. Conclusions

The complete flow field has been solved along with conjugate heat and mass transfer corresponding to the drying of a rectangular brick. The results show that the leading edge dries faster, as compared to other regions. It is also observed that two-dimensional results differ significantly from the predictions of one-dimensional heat and mass transfer coupled with boundary layer approximations over the top surface especially in the regions away from the leading edge. It is also demonstrated that heat and mass transfer coefficients based on constant temperature and moisture potentials may be more representative of the conjugate heat and mass transfer processes during drying, than those based on instantaneous ΔT and ΔC. The flow due to buoyant forces can be a significant external transport mechanism and must be taken into account for low Reynolds numbers.

References

[1] A.V. Luikov, Heat and mass transfer in capillary porous bodies, Pergamon, New York, 1966.
[2] S. Whitaker, Simultaneous heat, mass and momentum transfer – a theory of drying, Adv. Heat Transfer 13 (1977) 119–203.
[3] S. Ben Nasrallah, P. Perre, Detailed study of a model of heat and mass transfer during convective drying of porous media, Int. J. Heat Mass Transfer 31 (5) (1988) 297–310.
[4] C.L.D. Huang, Multi-phase moisture transfer in porous media subjected to temperature gradient, Int. J. Heat Mass Transfer 22 (1979) 1295–1307.
[5] F. Kallel, N. Galanis, B. Perrin, R. Javelas, Effects of moisture on temperature during drying of consolidated porous materials, J. Heat Transfer ASME Trans. 115 (1993) 724–733.
[6] G. Comini, R.W. Lewis, A numerical solution of two-dimensional problems involving heat and mass transfer, Int. J. Heat Mass Transfer 19 (1976) 1387–1392.
[7] W.J. Ferguson, R.W. Lewis, A comparison of a fully non-linear and a partially non-linear heat and mass transfer analysis of a timber drying problem, In: Proceedings of the Seventh International Conference on Numerical Methods in Thermal Problems, vol. VII, Part 2, Stanford, 1991, pp. 973–984.
[8] A.A. Dolinsky, A.Sh. Dorfman, B.V. Davydenko, Conjugate heat and mass transfer in continuous process of convective drying, Int. J. Heat Mass Transfer 34 (11) (1991) 2883–2889.
[9] W. Masmoudi, M. Prat, Heat and mass transfer between a porous medium and a parallel external flow. Application to drying of capillary porous materials, Int. J. Heat Mass Transfer 34 (8) (1991) 1975–1989.
[10] B. Zeghmati, M. Daguenet, Study of laminar free convection over an inclined wet flat plate, Int. J. Heat Mass Transfer 34 (4/5) (1991) 899–909.
[11] S. Oliveira Leandro, Haghighi Kamyar, Conjugate/adaptive finite element analysis of convective drying problem, In: Proceedings of the Ninth International Conference on Numerical Methods in Thermal Problems, vol. IX, Part 2, Atlanta, 1995, pp. 80–88.
[12] B.S.V.P. Patnaik, K.N. Seetharamu, P.A. Aswatha Narayana, Simulation of laminar confined flow past a circular cylinder with integral wake splitter involving heat transfer, Int. Num. Meth. Heat Fluid Flow 6 (1996) 65–81.
[13] Mauri Fortes, M.R. Okos, Heat and mass transfer in hygroscopic capillary extruded products, AIChE J. 27 (1981) 255–262.
[14] Chien-Tung Yang, S.N. Atluri, An assumed deviatoric stress–pressure–velocity mixed finite element method for unsteady, convective, incompressible viscous flow: Part II: computational studies, Int. J. Num. Meth. Fluids 4 (1984) 43–69.
[15] K. Murugesan, K.N. Seetharamu, P.A. Aswatha Narayana, A one-dimensional analysis of convective drying of porous materials, Heat Mass Transfer 32 (1996) 81–88.
[16] B. Perrin, R. Javelas, Transferts couples de chaleur et de masse dans des materiaux consolides utilises en genie civil, Int. J. Heat Mass Transfer 30 (2) (1987) 297–309.